Universität Potsdam

Kai-Uwe Thiessenhusen, Larry W. Esposito,
Jürgen Kurths, Frank Spahn

Detection of hidden resonances in Saturn‘s B-Ring

NLD Preprints ; 13

Detection of Hidden Resonances in Saturn's B-Ring

Kai-Uwe Thiessenhusen
Working group "Nonlinear Dynamics" (MPG)
University Potsdam; D-14115 Potsdam; Germany

Larry W. Esposito
University of Colorado at Boulder,
Laboratory for Atmospheric and Space Physics,
Boulder, Colorado 80309-0392

Jürgen Kurths
Working group "Nonlinear Dynamics" (MPG)
University Potsdam; D-14115 Potsdam; Germany

Frank Spahn
Working group "Nonlinear Dynamics" (MPG)
University Potsdam; D-14115 Potsdam; Germany

Keywords: Planetary Rings
Number of pages: 30
Number of figures: 8

Proposed Running Title:
Hidden Resonances in Saturn's B-Ring

Corresponding address:
K. Thiessenhusen
AG "Nichtlineare Dynamik", Uni Potsdam
Am Neuen Palais, Haus 19
Postfach 601553
14415 Potsdam
Germany

e-mail
kut@rz.uni-potsdam.de

Phone: (49)-331-977-1611
Fax: (49)-331-977-1142

Abstract

The Voyager 2 Photopolarimeter experiment has yielded the highest resolved data of Saturn's rings, exhibiting a wide variety of features. The B-ring region between 105000 km and 110000 km distance from Saturn has been investigated. It has a high matter density and contains no significant features visible by eye. Analysis with statistical methods has led us to the detection of two significant events. These features are correlated with the inner 3:2 resonances of the F-ring shepherd satellites Pandora and Prometheus, and may be evidence of large ring particles caught in the corotation resonances.

1 Introduction

The Voyager occultation experiments have yielded a great variety of structures in Saturn's rings. The photopolarimeter data (PPS, Lane *et al.* 1982, Esposito *et al.* , 1983a) exhibit structures at all length scales until the resolution limit of the data ($\approx$ 100 m).

A number of previous papers relate these observed features to physical processes, such as resonant effects, self gravity, or ballistic and collisional transport. Among them, there are compilations about all known resonant effects given by Lissauer and Cuzzi (1982) and Holberg *et al.* (1982). More generally, Esposito *et al.* (1987) have listed statistically significant events in the rings by means of a Student's t-test. They have found 216 features in the rings.

Following their investigations, we have analyzed the B-ring region between 105000 km and 110000 km radial distance from Saturn's center where no significant features have yet been found. It should be noted that this region is the longest one in the rings where no significant effects had been detected in all occultation experiments until now. The observed fluctuations seem to be noisy and do not change their characteristics throughout the whole region.

This region is flanked by zones where strong irregular fluctuations have been observed (e.g. Esposito *et al.* , 1986). Thus, understanding of the fluctuations in that region could provide a base in order to explain the effects in the neighboring zones. Additionally, the knowledge of how these small fluctuations arise in a region with very small perturbations, could give important hints for the understanding of the behavior of dense ring matter in similar regions.

Unfortunately, the high matter density in the studied region leads to a low photon count rate in the occultation experiment, i.e. the signal to noise ratio in this region is very small. In addition, most of the detected photons result from light scattered from Saturn's surface or other parts of the ring, and not from the occulted star (Esposito *et al.* , 1983).

Therefore, a crucial point of the analysis is whether the interesting characteristics of the data received at the experiment are due to background or other observational effects or whether they contain information about the investigated ring region itself. In the latter case it must be answered whether there are only random fluctuations or some kind of deterministic behavior,

such as long-range effects.

For this purpose, we use some refined statistical techniques which permit us to decide whether the data contain more information than only background effects.

The paper is organized as follows: In section 2 we describe the character of the analyzed data, section 3 deals with the features detected in the applied tests and with their correlation to resonances, and the conclusions are summarized in section 4.

2 The Data

The studied region is located in the central B-ring approximately between 105000 km and 110000 km from Saturn's center. There are no obvious visible features in this region. The inside and outside adjoining areas are characterized by the appearance of strong irregular fluctuations. For context see Figures 2 and 8 in Esposito *et al.* (1984) and the plots in the atlas of Saturn's rings by Collins *et al.* (1983).

Figure 1 shows a density profile through the B-Ring, where the optical depth τ - a measure for the matter density - obtained from the PPS data has been plotted against the radius.

The Voyager photopolarimeter (PPS) data consists of the measured intensity values of the star δ Scorpii occulted by the ring particles as a function of the distance from Saturn. The denser the ring matter at the position between space probe and star, the less the detected amount of photon counts.

The relation between measured intensity and the optical depth τ i.e. the matter density is given by (Esposito *et al.* 1983a)

$$\tau = cos\theta \;\; ln\frac{I_o}{I-B} \tag{1}$$

with
τ - optical depth,
I - measured intensity,
I_o - intensity of the unocculted star,
B - amount of background photons

θ- incidence angle relative to the ring plane normal.

In the PPS-experiment, θ was approximately 61.3 degrees and I_o was 39 counts.

The high optical depth in the observed region causes a small signal intensity so that fluctuations make the signal to noise ratio very low. The measured photon count rate is fluctuating around an average intensity value of 11 counts. The photon count distribution can be assumed as a Poissonian. The amount of background photons can only estimated. Esposito *et al.* (1983a, 1987) inferred a value near 10 which is only slightly smaller than the average photon count rate.

Figure 2 shows a typical sector within the studied region. The original, observed photon counts are plotted as a function of the radial distance from Saturn.

The major part of the measured photon counts is due to scattered light from other ring regions or from Saturn's disk. The actual amount of this background signal is not exactly determined. However, it can be assumed that such effects are constant over relatively long length scales. Thus, the structures caused by the fluctuations of the surface density of ring matter should be distinguished from backscattered light, or at minimum they should not be influenced very much by slow changes in scattered light.

To avoid systematic errors due to the unknown amount of background effects we restrict our analysis to the original photon counts. The data are then a spatial series with a resolution of approximately 100 m.

Figure 3 shows the radial variation of some main statistical short term parameters (mean value, standard deviation) derived from the data. In our example, all these values have been computed as the average values over a sliding interval of 500 points. We find them exhibiting only small changes within the studied region between 105 000 and 110 000 km .

The systematical search for features in Saturn's rings by Esposito *et al.* (1987) was restricted to a Student's t-test for the mean photon count values. The deviations in the mean values are too small over this whole region to become significant in that test.

It cannot be distinguished by means of the above tests whether the apparent fluctuations are due to the conditions of the experiment or whether they contain information about the physical behavior of ring matter. Nor can we distinguish between short range structures (below the resolution limit) and

noise. In order to clarify the nature of the measured data, further tests are presented in the following section.

3 The Methods and their Results

As mentioned above, we refer in our tests to the raw PPS occultation counts only, because any calculation of the optical depth gives an additional systematic uncertainty due to the unknown background effects. We assume that these effects are slowly varying with the distance, and that they do not influence the applied tests.

3.1 Chi- Square Test

We have modified a special χ^2 - test developed by Isliker and Kurths (1993) as a test for stationarity. In our test the photon count intensity distribution of a short interval is compared with that one of its surrounding. Then the narrow sample window is scanned over the entire region considered.

The distributions are formed by the numbers of photon counts of different intensity classes. The χ^2- values are given by

$$\chi^2 = \sum_{i=1}^{k} \frac{(M_i - Np_i)^2}{Np_i} \tag{2}$$

with
k -number of classes
M_i - number of sample points in the class i
N - number of sample points
p_i - relative frequency for the class i in the surrounding

As a measure for the deviation of the sample from its surrounding, we have displayed χ^2 as a function of the radial distance from Saturn. The lengths of the test intervals as a well as the classification of the counts have been varied in order to determine influences of the chosen parameters.

In our example (Fig. 4), the distribution of a 500 points (52.6 km) sample has been compared with the 15000 points long region surrounding it (including the sample). The sample is located in the center of the surrounding region. In our example, the photon count values have been divided into 17 classes. The first class contains all counts <7, each count from 7 up to 21 corresponds with class 2 up to 16, and the last class contains all counts > 21. If the features have sizes on the order of the sample length, the sensitivity to the relative positions between the feature and the sample window may be high. We have overlapped the sample windows in order to reduce this sensitivity. The distance between two adjacent samples is 150 data points, giving an overlap of 350 points.

Two significant peaks occur for a broad range of the selected test parameters, i.e. for sample windows large enough (> 10 km) to avoid the influence of short range fluctuations and not too large (< 100 km) that the features will not vanish in the surrounding noise. This could be an estimate for the sizes of the features.

The features are located approximately at 106450 km and at 108150 km radial distance from Saturn. The accuracy of the position estimation is limited by the window length so that a systematic position error of 50 km must be taken into account for Figure 4.

Depending on the number of degrees of freedom (number of classes - 1), each χ^2 - value corresponds with a probability that the value can be reached by chance. In our example, the peaks have χ^2 - values of 70 and 56 respectively. The corresponding probability for a random realization of a χ^2 - value of 56 is lower than 0.00001, for 70 still much lower. The probability to have one such event purely by chance in a number of events depends on this number. In this example, for a sample distance of 150 points, the number of calculated χ^2 - values in the region is 316. The corresponding probability p for one random event is lower than $1-(1-0.00001)^{316} = 0.31\%$ and for two of such events lower than p^2.

3.2 m -Test

We have compared the above results with those of another statistical test, which has been applied by Colwell *et al.* (1990) for the detection of small rings in the Uranian system. The photon count distribution can be approximated as a Poisson distribution, characterized by the mean value μ as the

only parameter. The standard deviation σ equals $\sqrt{\mu}$. In the discrete case, the probability P_I for detecting a counting rate I in a region with the mean photon count value μ is given by

$$P_I(I,\mu) = \frac{e^{-\mu}\mu^I}{I!} \tag{3}$$

Thus, the probabilities $P_H(C,\mu)$ for getting a counting rate $\geq C$ and $P_L(C,\mu)$ for a rate $\leq C$ are

$$P_H(C,\mu) = 1 - \sum_{I=0}^{C-1} \frac{e^{-\mu}\mu^I}{I!} \tag{4}$$

$$P_L(C,\mu) = \sum_{I=0}^{C} \frac{e^{-\mu}\mu^I}{I!} \tag{5}$$

Now, we define

$$m_H(C,\mu) = n(1 - \sum_{I=0}^{C-1} \frac{e^{-\mu}\mu^I}{I!}) \tag{6}$$

and

$$m_L(C,\mu) = n \sum_{I=0}^{C} \frac{e^{-\mu}\mu^I}{I!} \tag{7}$$

The values m_H and m_L represent the expectation values for the number of events with a counting rate $\geq$ C respectively $\leq$ C in an ensemble with n Poissonian distributed values. In the purely random case, the expectation value for the numbers of events with an m - value of about 1 is just 1.

With the m-test, high and low count rates can be considered separately. Figure 5 shows the m_H-values as a function of the distance from Saturn. In this example, we have chosen the same parameters as in the chi-square test. The data have been binned 500 times so that each intensity value C represents an approximately 52.6 km long region. The distance between two neighbored samples has been 150 data points. The normalized mean photon count value μ has been derived from the 15000 data points long surrounding. In order to visualize deviations from the Poissonian distribution which are characterized by extremely small m - values, we have plotted (Fig. 5) the m_H (C,μ) - values on a logarithmic scale. Again, two features with extremely low m_h - values occur at the same positions as of the significant features in the χ^2 - test. The m_h -values at the peaks are about 0.001. That means that photon count rates as at the peak positions can be expected once in thousand purely random realizations. Again, the probability for the occurrence of two of such deviations is much smaller. At the locations of the detected features, there is an increase of the photon count rate by 0.3 - 0.4 counts over a length of about 30 km.

With the m_L test, no comparable features have been detected.

3.3 Correlation with Resonances

To find out the nature of processes forming the detected features we have tested a correlation with resonances.

For the calculation of the resonant positions we follow e.g. Goldreich and Tremaine, 1980; Shu, 1984.

The two resonances with the distinctly strongest torques in the region are the 3:2 resonances of the F-ring shepherd satellites Prometheus and Pandora. Other resonances of these satellites are responsible for several features in the A-ring. The approximated positions of the inner 3:2 resonances are for the Lindblad resonances are 108545 km for Pandora and 106771 km for Prometheus, and for the vertical resonances 107985 km and 106187 km.

The events detected in the tests have positions relative to the resonances that are very similar for both cases.

The observed features are located very close to the positions of the corotational resonances - just at the resonance position of Prometheus and just a bit inside that of Pandora between the inner 3:2 Lindblad and the corresponding vertical resonances. Due to the results of the two statistical tests it

can be excluded with a high probability that the observed features are of random origin. Furthermore, the probability that the two distinctly strongest features appear by chance closely to the two strongest resonances is small too. Assuming two 700 km long intervals where effects due to the 3:2 resonances of Prometheus and Pandora could appear, the probability for a random positioning of the two features in these intervals out of a 5000 km long region is about 4%. If one takes into account that both features are almost at the similar positions relative to the resonances, this probability becomes even smaller.

Typical resonant features can cause depletions in the observed optical depth at the resonance positions, with density waves propagating radially outward from the Lindblad resonances and bending waves radially inward from the vertical ones. The effects due to the vertical resonances are expected to be small in this case. In these tests, no significant features at the positions of density or bending waves could be observed. Due to the high background intensity, even high density fluctuations change the photon count rate only slightly. Such fluctuations could not been distinguished from noise by means of the tests described above. Relatively broad depletions can be detected much easier.

A physical explanation for these effects still must be given. Corotational resonances are not predicted to have a great influence on the matter density in the rings. One exception are wave-like features at the 2:1 resonance of Janus (Goldreich and Tremaine, 1979). Molnar *et al.* (1994) have explained a large depletion in the optical depth further outward in the B-ring by the 2:1 corotational resonance of Mimas.

We propose as a possible explanation gravitational stirring of smaller ring particles due to one or more larger ones trapped at the resonant positions (for resonant trapping see e.g. Sicardy 1992). In this case, although the larger ring particles may not be big enough to clear a gap (Henon 1981) they can produce local density variations and decrease the mean opacity. This would naturally explain the results of the χ^2 - and m -tests near the corotation locations.

3.4 Comparison with Imaging Data

Beside the described tests, a comparison with independently gained data is of interest. All occultation data suffer from low light intensity in regions with high density, but this is not the case for light scattering experiments. These imaging data have a much lower resolution than the PPS data and are sensitive to surface properties of the ring material.

Figure 6 shows an imaging profile of light reflected at the rings. This green-filter imaging profile is the result of data analysis performed by Estrada and Cuzzi (1994). It is based on several narrow angle images by the Voyager-probes.

In figure 6, the normalized intensity I/F of the reflected light has been plotted against the radial distance from Saturn. An I/F value of 1 corresponds to an albedo of 1 and a scattering angle of 0 °. The spatial resolution of the data is about 12 km.

The intensity values in the data show an increasing tendency from 105 000 km up to 109 000 km. This increase may be due to a change of color or brightness of the ring material.

There seems to be no obvious correlation to the PPS-features, but the elimination of the long-ranged tendencies in the images leads to a different result (Figure 7). In this example, the average intensity of the surrounding region has been subtracted from each data point. The length of this reference interval is with approximately 1560 km (130 data points) nearly the same as for the tests for the PPS - data described above. Two broad depletions can be seen at the resonance positions of Pandora and Prometheus which are marked with lines. Both features are quite similar, with full widths at half maximum of 400 - 500 km. The corresponding PPS features are much narrower, i.e., only the zones of the lowest intensity within these depletions cause significant changes in the PPS-data. The minima in the optical data are at 106 480 km and at 108 160 km. These positions are the same as those of the detected PPS-features, taking into account a resolution of 12 km for this data and an uncertainty of about 30 km due to the window length in the PPS-data analysis. Beside this, some wave - like features outside the Lindblad resonance of Prometheus which could be due to density waves are slightly visible in the imaging data.

The comparison between the imaging data and the χ^2 test is displayed

in Figure 8. χ^2-values < 25 which are not above the noise level and density enhancements in the optical data (Δ I/F > 0) are not plotted in this picture. The features in the χ^2 test are in good accordance with the minima of the broad depletions in the intensity profile of scattered light.

Thus, the optical data seem to reinforce the results of the PPS-data analysis. The location of the PPS-features are in good accordance with those shown in the optical data.

4 Conclusion

We have analyzed the B-ring region between 105000 km and 110000 km distance from Saturn where no significant structures in the Voyager occultation data were reported until now. The analyzed occultation data are strongly influenced by background effects, leading to a low signal - to - noise ratio.

With special techniques, two significant features have been found in these rather homogeneous looking data. Their locations are close to the 3:2 resonances of Pandora and Prometheus and thus make a correlation to these resonances probable. These resonances are those with the distinctly highest torques of all resonances occurring in the studied region.

The finding of these features supports the conclusion that the studied PPS data contain physical information about the ring matter beside background effects. The tests described above have been straightforward, simply seeking differences from a purely random signal. Perhaps, further analysis with more sophisticated methods may also be worthwhile. More detailed investigations could determine whether density or bending waves exist there at the calculated resonance positions, which could not been detected in this study. A further comparison with the analysis of data gained from the optical experiments could be useful in order to make a new systematic analysis of all ring features in extension of the work of Esposito *et al.* 1987.

Beside this, the search for a physical explanation for the detected features is necessary. Our immediate proposal is, that there is a significant probability that large ring particles or small moonlets can be captured near the corotational resonance positions. These bodies enhance the velocity dispersion of smaller particles near their orbits so that a depletion of the optical depth can be observed at these positions.

Acknowledgement

The authors would like to thank Paul Estrada and Jeff Cuzzi for providing us with the imaging data, and Mark R. Showalter for his support in this field. We also wish to thank Linda J. Horn and an anonymous referee for helpful comments.

This work has been supported by the Deutsche Forschungsgemeinschaft (*DFG*).

References

Collins S.A, J. Diner, G.W. Garneau, A.W. Lane, E.D. Mine., S.P. Synnott, R.J. Terrile, J.B. Holberg., B.A. Smith, G.L. Tyler 1984. Atlas of Saturn's Rings. In *Planetary Rings,* Eds. R.Greenberg and A.Brahic, Univ. of Arizona Press, Tucson, 737–743.

Colwell, J.E., L.J. Horn, A.L. Lane, L.W. Esposito, P.A. Yanamandra - Fisher, S.H. Pilorz, K.E. Simmons, M.D. Morrison, C.W. Hord, R.M. Nelson, B.D. Wallis, R.A. West and B.J. Burratti 1990. Voyager photopolarimeter observations of Uranian ring occultations. *Icarus* **83,** 102–125.

Esposito, L.W, M. O'Callahan, K.E. Simmons, C.W. Hord, R. A. West.A.L. Lane, R.B. Pomphrey, D.L. Coffeen and M. Sato 1983a. Voyager photopolarimeter stellar occultation of Saturn's rings. *J. Geophys. Res.* **88,** 8643–8649.

Esposito, L.W, M. O'Callahan and R.A. West 1983b. The structure of Saturn's rings: implications from the Voyager stellar occultations. *Icarus* **56,** 439–452.

Esposito, L.W., J.N. Cuzzi, J.B. Holberg, E.A. Marouf, G.L. Tyler, C.C. Porco 1984. Saturn's rings: structure, dynamics, and particle properties. In *Saturn,* Eds. T.Gehrels and M.S. Matthews, Univ. of Arizona Press, Tucson, 463–545.

Esposito, L.W., C.C. Harris and K.E. Simmons 1987. Features in Saturn's rings. *The Astroph. J. Supp.* **63,** 749–770.

Estrada,P. and J. N. Cuzzi 1994. . *submitted to Icarus.*

Goldreich,P.and S. Tremaine 1979. The excitation of density waves at the Lindblad and corotational resonances by an external potential. *Astrophys. J.* **233,** 857–871 .

Goldreich,P.and S. Tremaine 1980. Disk Satellite Interactions. *Astrophys. J.* **241 ,** 425–441 .

Henon, M 1981. A simple model of Saturn's rings. *Nature* **293,** 33–35.

Holberg, J. 1982. Identification of 1980S27A and 1980S26A resonances in Saturn's A-Ring. *Astron. J.* **87,** 1416–1422.

Holberg, J., W.T. Forrester, and J.J. Lissauer 1982. Identification of resonance features with the rings of Saturn. *Nature* **297,** 115–120.

Isliker H.and J. Kurths 1993. A test for stationarity: Finding parts in time series apt for correlation dimension estimation. *Int. J. of Bif. and Chaos* **3,** 1573–1579.

Lane, A.L., C.W. Hord, R.A. West, L.W. Esposito, L.W., D.L. Coffeen, Sato, M., K.E. Simmons, R.B. Pomphrey, and R.B. Morris 1982. Photopolarimetry from Voyager 2: preliminary results on Saturn, Titan and the rings. *Science* **215,** 537–543.

Lissauer, J.J.and J.N.Cuzzi 1982. Resonances in Saturn's rings. *Astron. J.* **87,** 1051–1058.

Molnar, L.A, and L. Dunn 1994. The Mimas 2:1 eccentric corotational resonance. in preparation

Sicardy, B. 1991. Numerical explanation of planetary arcs. *Icarus* **89,** 197–219.

Shu, F. 1984. Waves in Saturn's rings . In *Planetary Rings,* Eds. R.Greenberg and A.Brahic, Univ. of Arizona Press, Tucson, 513–561.

Figure Captions

Fig. 1: B-Ring density profile.

The x-axis is the radial distance from Saturn, the y-axis the optical depth.

Fig. 2: Part of the studied region

The x-axis is the radial distance from Saturn, the y-axis are the photon count values of the PPS-data. The resolution is about 100 m.

There are no clearly visible features except for short scale fluctuations.

Fig. 3: Part of B-Ring

The x-axis is the radial distance from Saturn, the y-axis are the photon counts. This picture shows the values of the mean photon count values n (upper curve) and the standard deviation σ (lower curve). Each value has been computed over 500 data points. There are no clearly visible features in the region between 105 000 km and 110 000 km.

Fig. 4: χ^2- test of the PPS-data

The x-axis is the radial distance from Saturn, the y-axis are the χ^2-values. The photon count distribution of an 500 data points (approximately 52.6 km) region has been compared with that of the 15000 data points surrounding it by an χ^2- test. The distance between two displayed points is 150 data points.

There are two significant deviations observed. The χ^2-values at the peaks correlate with a probability that each of them is of random origin of lower than 0.00001. The resonance positions of the 3:2 resonances of the F-ring shepherds Prometheus and Pandora are marked.

Fig. 5 m - test of the PPS-data

The x-axis is the radial distance from Saturn, the y-axis are the m-values on a logarithmic scale. There are two deviations at the same positions as in the χ^2-test. The m-values are a measure for the deviation of the averaged photon count rate of a 500 data points long sample from that of its 15000 points long surrounding. The distance between two samples is 150 data points. There are two large deviations at the same

positions as in the χ^2-test. The m-values of about 0.001 at these peaks express that photon count rates as at these positions can be expected only once in thousand random realizations.

Fig. 6 Voyager imaging data.

The x-axis is the radial distance from Saturn. The y-axis shows a normalized intensity profile I/F of light scattered at the rings. The nominal resolution is about 12 km.

Fig. 7 Detrended imaging data

The x-axis is the radial distance from Saturn, the y-axis shows the local intensity changes Δ I/F.

The average value of on approximately 1500 km surrounding has been subtracted from each data point. The resolution is the same as in Fig. 6. Two broad depletions occur at the resonance positions which are marked with lines.

Fig.8 Comparison of the chi-square features in the PPS data with the detrended optical data. The x-axis is the radial distance from Saturn. Upper Half: The y-axis are the chi-square values as in Fig. 4. Chi-square values lower than 25 are not displayed.

Lower Half: Detrended intensity profile as in Fig. 7. The y-axis shows the local intensity changes Δ I/F. Intensity enhancements (Δ I/F >0) - which are not detectable in the PPS-data are not displayed.

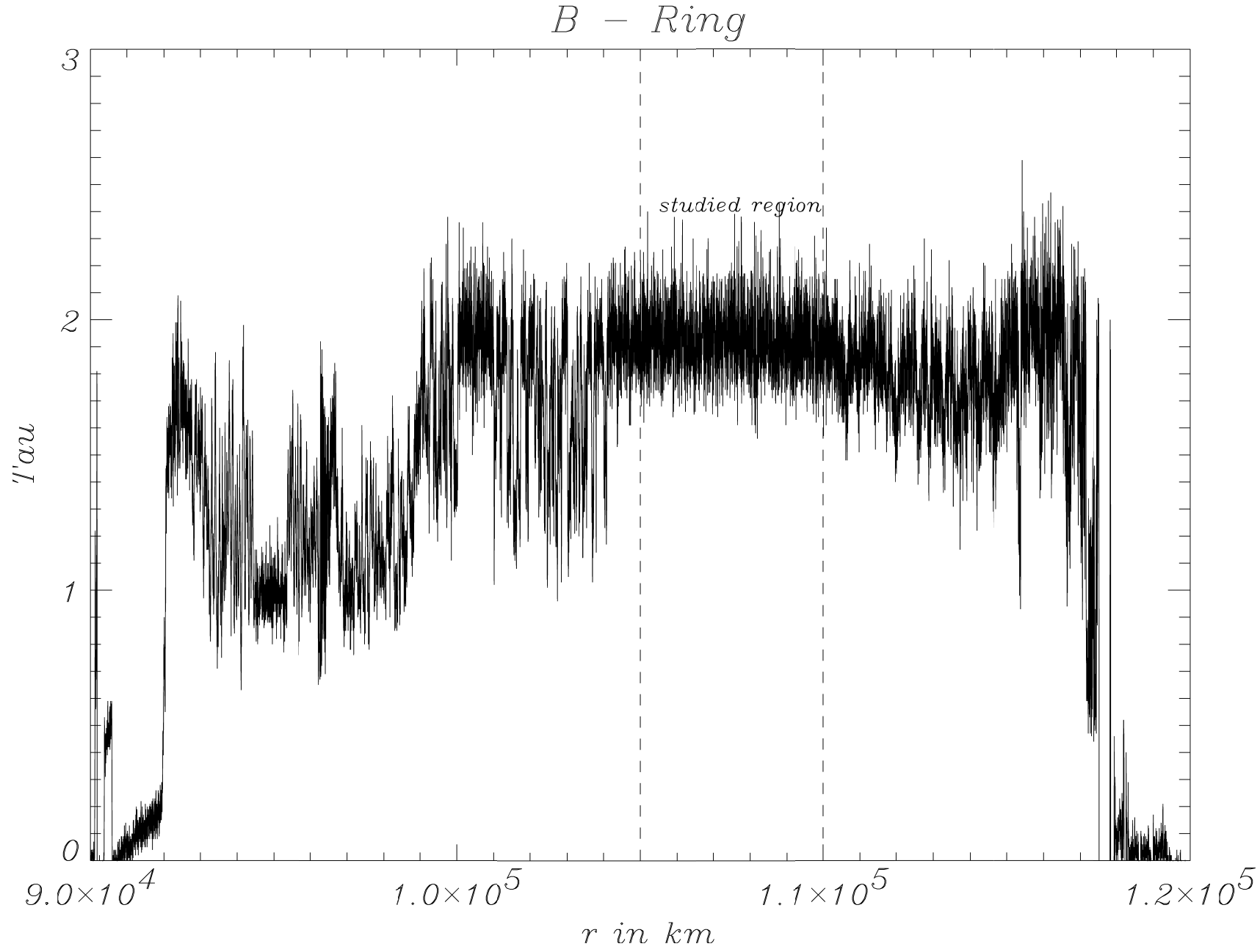
B − Ring
studied region
τ'au
0
1
2
3
9.0×10^4
1.0×10^5
1.1×10^5
1.2×10^5
r in km

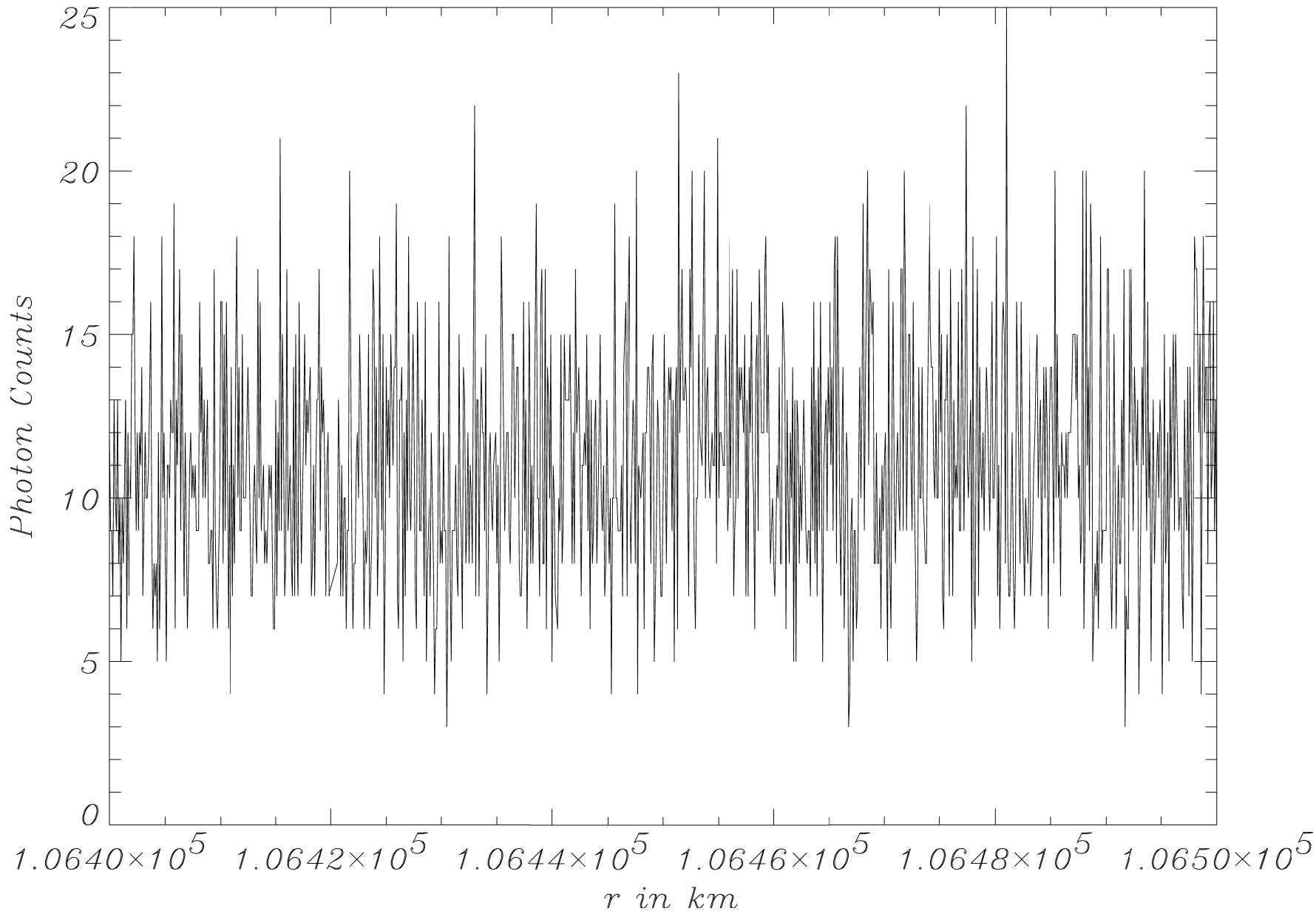
25
20
15
10
5
0
Photon Counts
1.0640×10^5
1.0642×10^5
1.0644×10^5
1.0646×10^5
1.0648×10^5
1.0650×10^5
r in km

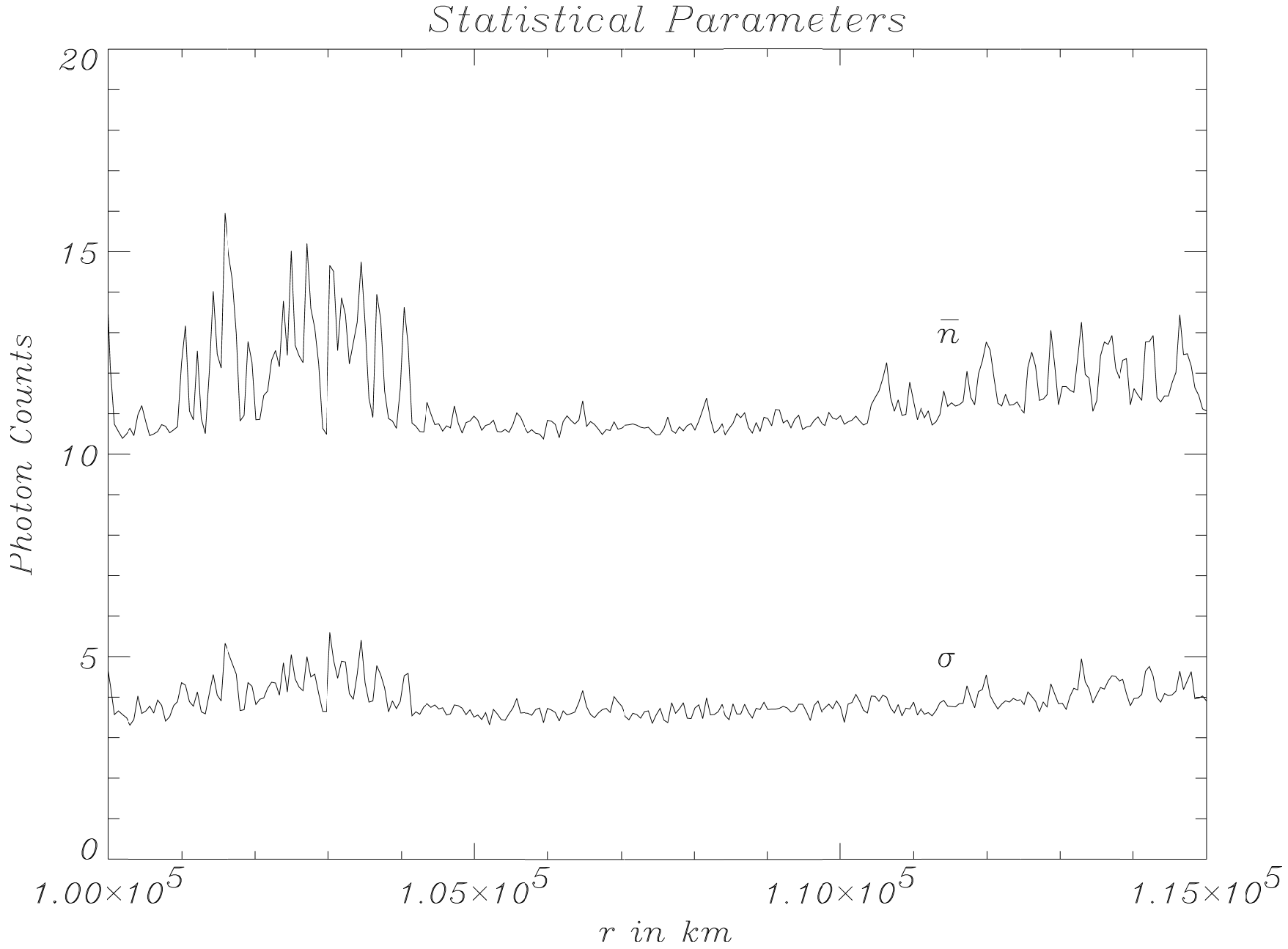
Statistical Parameters
20
15
10
5
0
Photon Counts
$\bar{n}$
σ
1.00×10^5
1.05×10^5
1.10×10^5
1.15×10^5
r in km

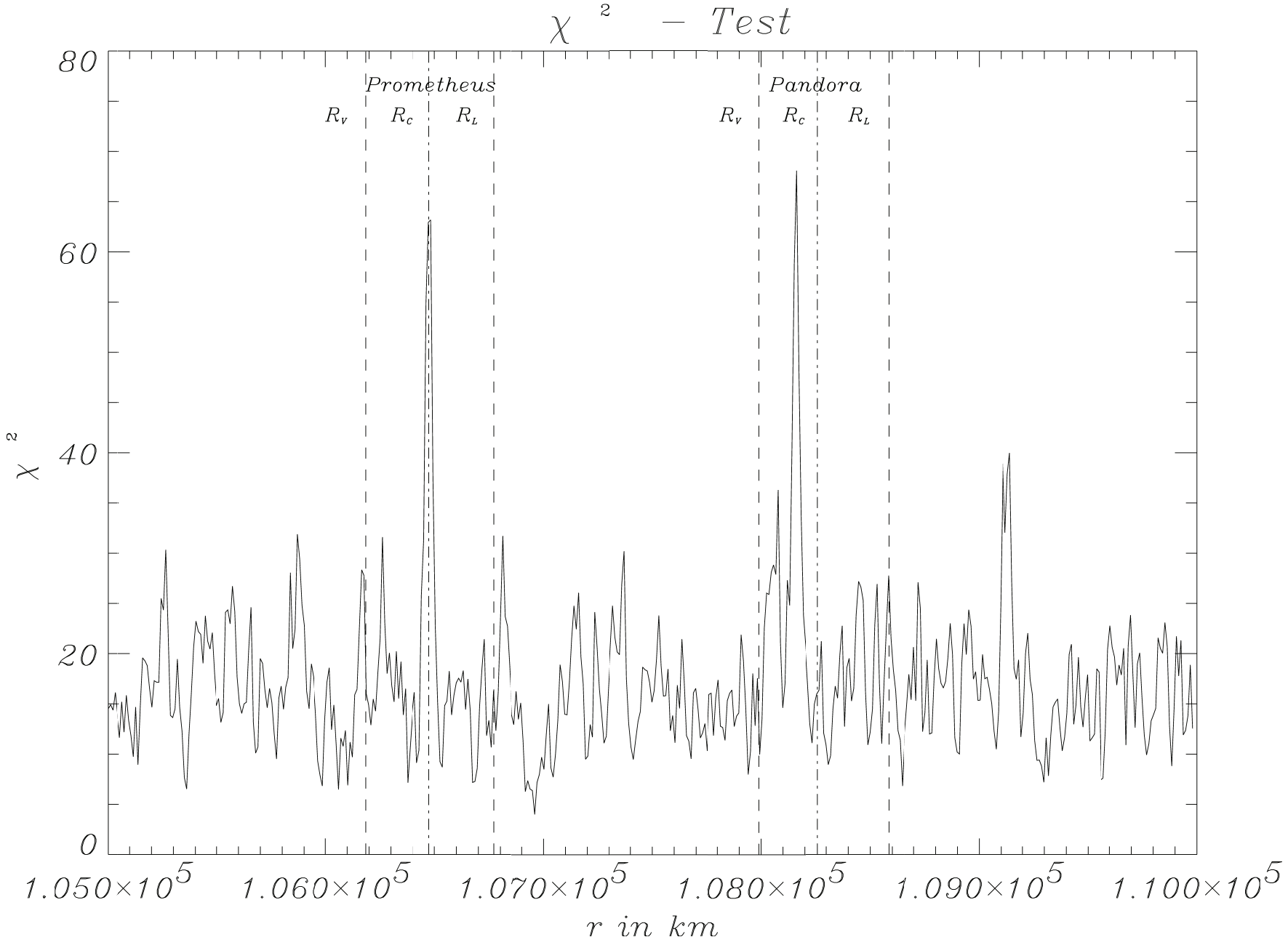
χ² − Test
Prometheus
Pandora
R_v
R_c
R_L
R_v
R_c
R_L
80
60
40
20
0
χ²
1.050×10^5
1.060×10^5
1.070×10^5
1.080×10^5
1.090×10^5
1.100×10^5
r in km

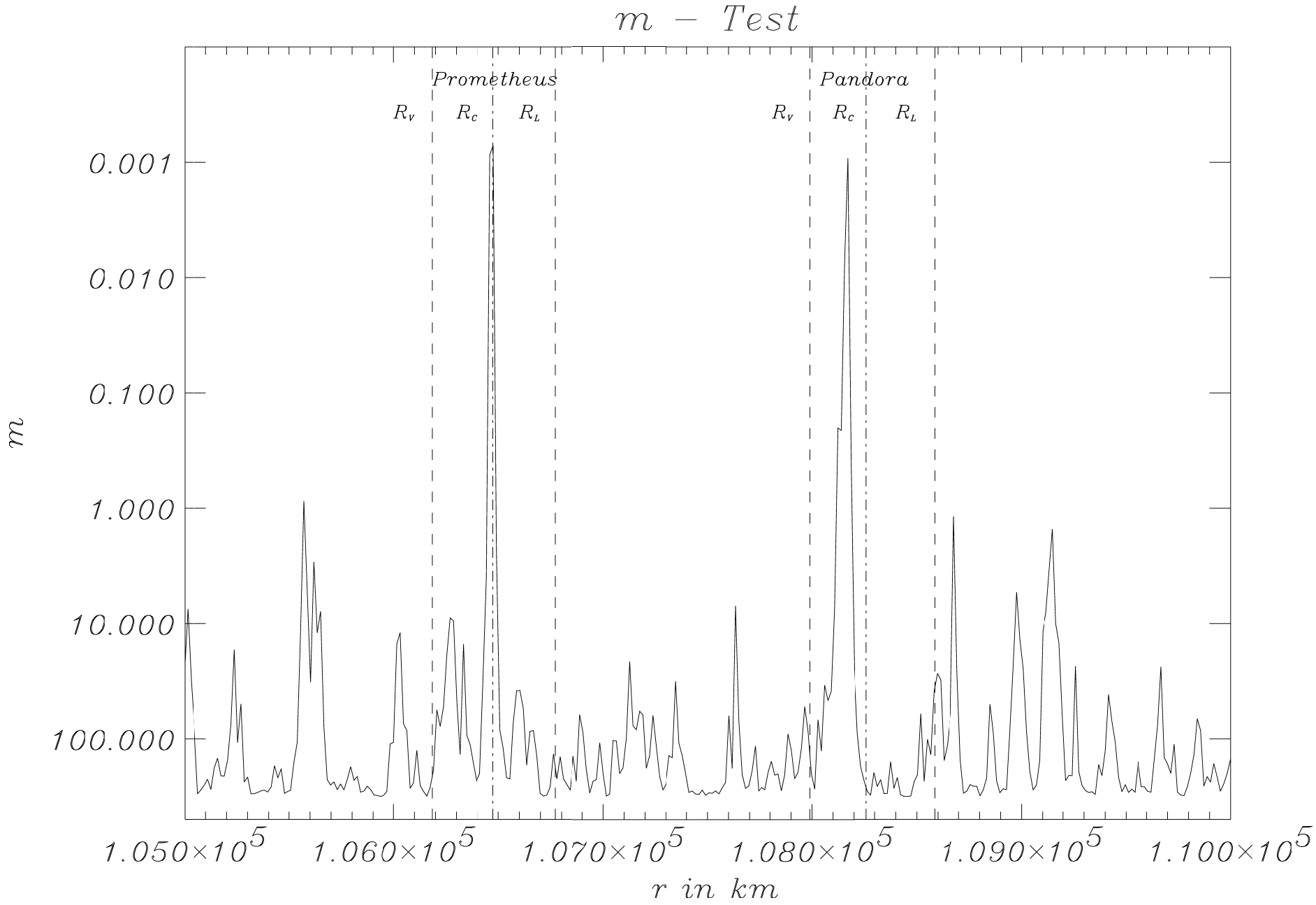
m − Test
Prometheus
Pandora
R_V
R_C
R_L
R_V
R_C
R_L
0.001
0.010
0.100
1.000
10.000
100.000
m
1.050×10^5
1.060×10^5
1.070×10^5
1.080×10^5
1.090×10^5
1.100×10^5
r in km


Imaging Data
0.30
0.28
0.26
0.24
0.22
0.20
I/F
1.050×10^5
1.060×10^5
1.070×10^5
1.080×10^5
1.090×10^5
1.100×10^5
r in km

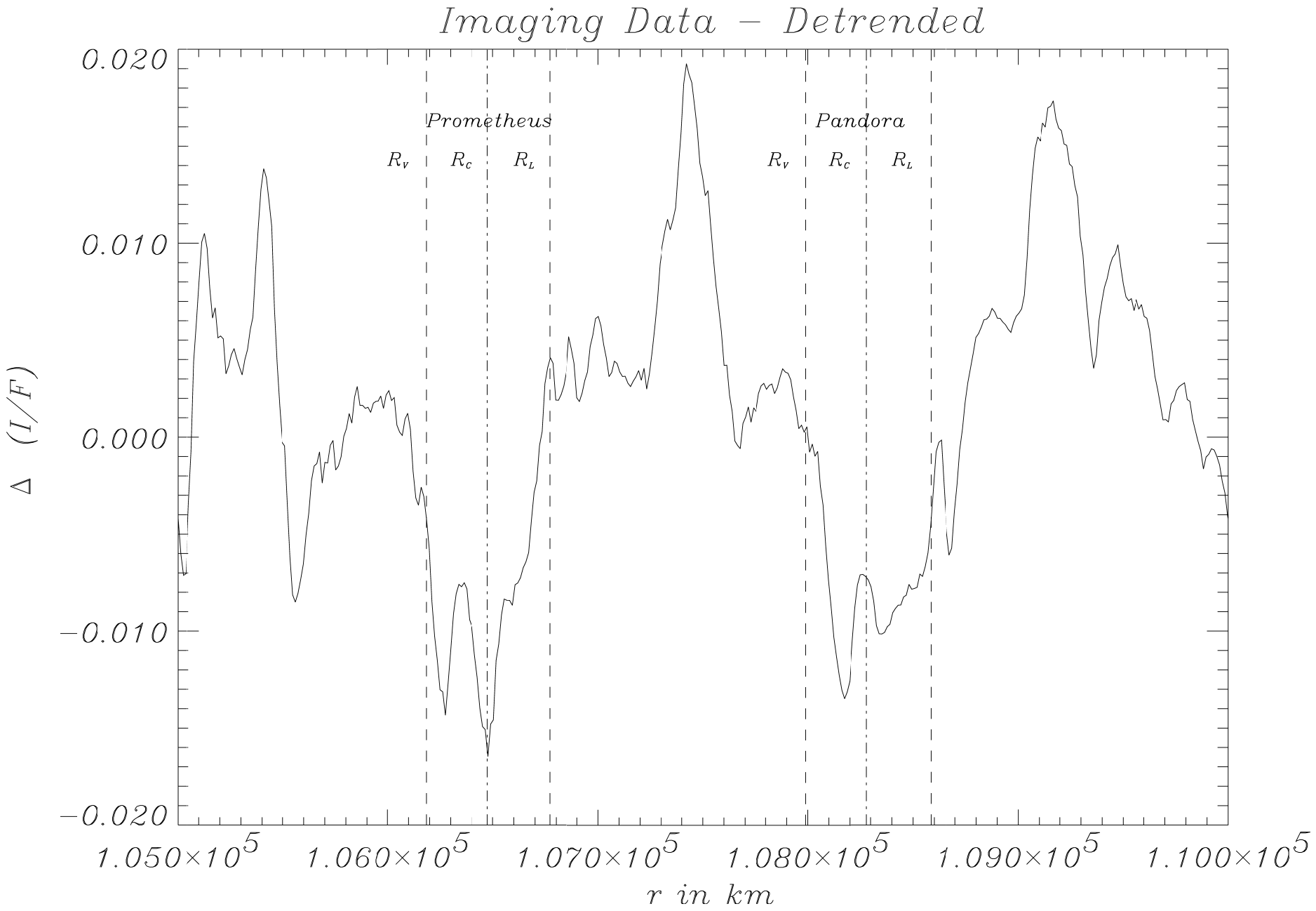
Imaging Data – Detrended
0.020
0.010
0.000
−0.010
−0.020
Δ (I/F)
Prometheus
Pandora
R_V
R_C
R_L
R_V
R_C
R_L
1.050×10^5
1.060×10^5
1.070×10^5
1.080×10^5
1.090×10^5
1.100×10^5
r in km

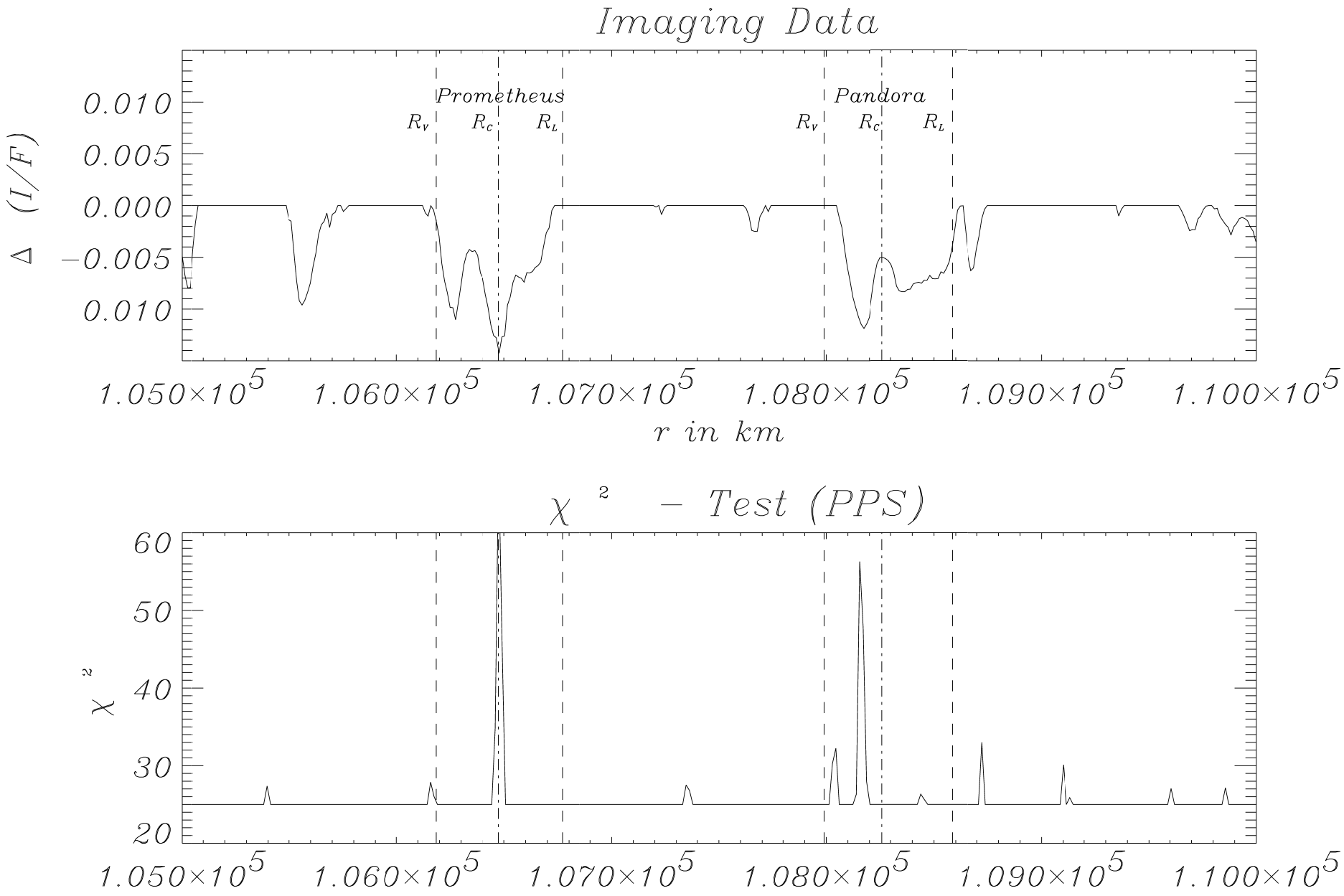
Imaging Data
Prometheus
Pandora
R_V
R_C
R_L
R_V
R_C
R_L
0.010
0.005
0.000
−0.005
0.010
Δ (I/F)
1.050×10^5
1.060×10^5
1.070×10^5
1.080×10^5
1.090×10^5
1.100×10^5
r in km
χ² − Test (PPS)
60
50
40
30
20
χ²
1.050×10^5
1.060×10^5
1.070×10^5
1.080×10^5
1.090×10^5
1.100×10^5